

Supplementary Material 1

Preparation of the Long Time Series Nighttime Light Data

1. DMSP-OLS Multisensory Data Correction

DMSP-OLS sensors have different sensitivities to nighttime illumination and experience different degrees of sensor degradation, and the DN values obtained from DMSP-OLS data are different within the same year for the different sensors or for the same sensor between different years [1]. Figure 1 shows the variation in the global nighttime light stable DN values from the F10 to F18 satellite sensors without mutual correction. Clearly, the uncorrected nighttime DN values at the global scale and the changes and differences at the annual scale are difficult to explain.

In 2017, Li and Zhou et al. [2] proposed a stepwise gradient calibration method for nighttime light data. Its principle involves the use of the data from multiple nighttime light data overlap periods as a reference for global calibration and the systematic correction of the DN values of a specific satellite or year exhibiting under- or overestimation. According to the method of Li et al., the authors obtained globally corrected lighting data from 1992 to 2013. After mutual correction, the temporal consistency of the different satellite lighting datasets was improved, and the changes in time series at the annual scale could also be reasonably explained from the perspective of economics (Figure S1).

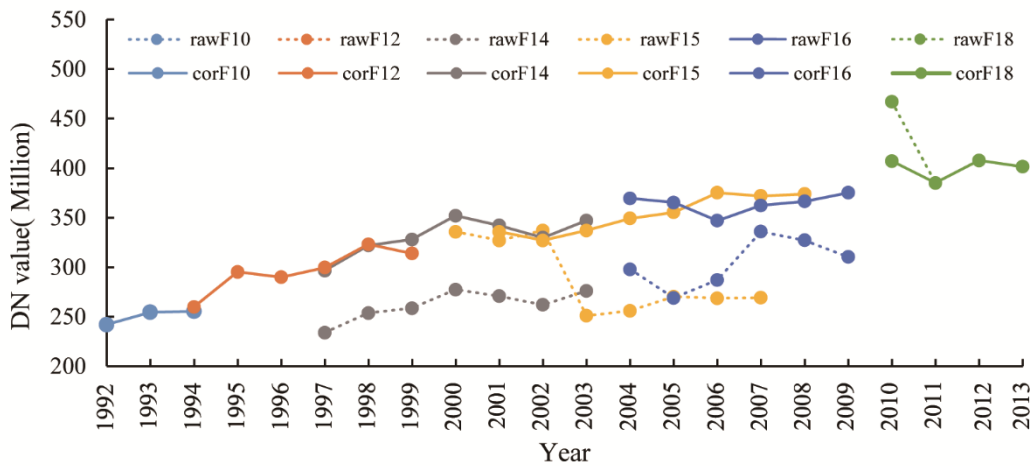


Figure S1. The annual sums of the DN values of the DMSP/OLS dataset before and after correction. The correction method proposed by Li and Zhou et al. [2] was applied to correct the DN values of the nighttime light data from the 6 different sensors (F10, F12, F14, F15, F16, and F18) in various years. After correction, the annual sum of the DN values exhibits reduced fluctuations between years and a higher consistency.

It is clearly shown in Figure S1 that in 1994 and from 1997–2007, there were at least two periods of stable light data acquired by the different sensors in each year. In the other years, there was only one sensor and one period of stable light data. According to the principle whereby the global-scale sum of the multisource nighttime light data DN values during the overlap period remains consistent, the deviation of the different years is visually the lowest, and the original NTL modification is maintained as small as possible. Hence, the authors successfully realized the preliminary correction of the DN sum of the different time series datasets. At the pixel scale, the annual DMSP-OLS data were corrected with the method of Liu et al. [3].

$$DN_{(n,i)} = \begin{cases} 0 & DN_{(n,i)}^a = 0 \text{ and } DN_{(n,i)}^b = 0 \\ DN_{(n,i)}^b \mid DN_{(n,i)}^a & DN_{(n,i)}^a = 0 \text{ or } DN_{(n,i)}^b = 0 \\ (DN_{(n,i)}^a + DN_{(n,i)}^b) / 2 & \text{other} \end{cases} \quad (1)$$

$n=1994, 1997, 1998, \dots, 2007$

where $DN_{(n,i)}$ is the i -th pixel DN value of the corrected n -th year image, and $DN_{(n,i)}^a$ and $DN_{(n,i)}^b$ are the i -th pixel DN values of the stable light image acquired by the different sensors after the n -th year correction.

2. NPP-VIIRS Data Preprocessing and Correction of the DMSP-OLS Data

The preprocessing approach of the NPP-VIIRS data includes 2 parts:

(1) Annual data decomposition. The NPP-VIIRS monthly composite data were decomposed into annual average composite nighttime light data. In the processing procedure, spatial matching with DMSP-OLS was considered, and the original 500-m resolution images were resampled to a resolution of 1 km by applying the nearest neighbor method.

(2) Generation of stable nighttime light data. The original NPP-VIIRS data include not only nighttime light data but also outliers such as fire points, volcanoes, and background noise. The NPP-VIIRS DNB nighttime light data contain negative DN value pixels and anomalous pixels with large DN values. First, using the 2015 and 2016 NPP-VIIRS annual synthetic data and the 2013 DMSP-OLS data provided by NASA to mask the NPP-VIIRS data of the other years, the spatial distribution of the stable nighttime light pixels was obtained. Thereafter, the DN pixel value when the cumulative pixel number reaches 99.9% was selected as the truncation threshold (the maximum value), and all DN values exceeding this threshold were replaced with the threshold value, thereby eliminating the few singular value pixels in the NPP-VIIRS dataset.

The processed annual NPP-VIIRS dataset must also be corrected to match the DMSP-OLS dataset. The principle is as follows: based on the spatial correspondence between the DMSP-OLS and NPP-VIIRS image data in the overlapping year (2013), a mathematical model is established via fitting for conversion purposes [4]. The authors experimented with a variety of mathematical models, including linear, quadratic, and exponential regression models, logarithmic models, etc., and finally adopted the exponential regression model. The specific model is defined as follows:

$$\begin{cases} x \leq x', & y = a \times x^b + c \\ x > x', & 63 \end{cases} \quad (2)$$

where x is the NPP-VIIRS value, y is the DMSP-OLS value, a , b , and c are coefficients, and x' is the threshold of model fitting. A comparison of the various mathematical simulations reveals that R^2 reached a maximum value of 0.65015 with the above regression model. The determination coefficients R^2 of the other models were 0.5360 (one-dimensional linear regression model), 0.6224 (quadratic linear regression model), and 0.5824 (logarithmic model).

3. Correction of the Time Series Data

It is generally believed that later DN values should be larger than, or equal to, previous DN values in the time series nighttime light dataset⁵. Based on this principle, Liu et al.³ proposed a method of logical verification and correction of time-series data, and after comparing two data periods, if a later DN value is smaller than the previous DN value, the later DN value is then assigned the maximum value. However, in specific regions and time periods, due to wars, abandonment of residential areas caused by economic downturn, closure of factories, etc., the above assumptions are not valid, and nighttime light index correction based on this principle will also cause significant deviations [6]. In general, the method of Liu et al. leads to the cumulative transmission defect of positive deviations [7].

To avoid the above problems, Zhao et al. [7] proposed a method consisting of simultaneously performing two logical tests and finally calculating the average value. First, a time-series data logic verification and correction process is executed involving a comparison of the data before and after two phases and selecting the maximum DN value in the later period. Second, a time-series data logic verification and correction process is performed by comparing the data before and after two phases and assigning the minimum value to the previous DN value. Finally, the above two correction values are averaged. Through the above processing steps, positive (the green line in **Error! Reference source not found.**) and negative (the red line in **Error! Reference source not found.**) deviations cancel each other. The corrected time series data (the orange line in **Error! Reference source not found.**) are objectively more in line with reality.

The specific equations for the correction are as follows:

$$DN1_{(n,i)} = \begin{cases} DN_{(n-1,i)} & DN_{(n,i)} < DN_{(n-1,i)} \\ DN_{(n,i)} & \text{other} \end{cases} \quad (n = 1993, \dots, 2013) \quad (3)$$

$$DN2_{(n,i)} = \begin{cases} DN_{(n+1,i)} & DN_{(n,i)} > DN_{(n+1,i)} \\ DN_{(n,i)} & \text{other} \end{cases} \quad (n = 1992, \dots, 2012) \quad (4)$$

$$DN_{(n,i)} = (DN1_{(n,i)} + DN2_{(n,i)}) / 2 \quad (n = 1992, \dots, 2013) \quad (5)$$

where $DN_{(n-1,i)}$, $DN_{(n,i)}$, and $DN_{(n+1,i)}$ are the i -th pixel DN values of the corrected images in the $(n-1)$ -th, n -th, and $(n+1)$ -th years, respectively.

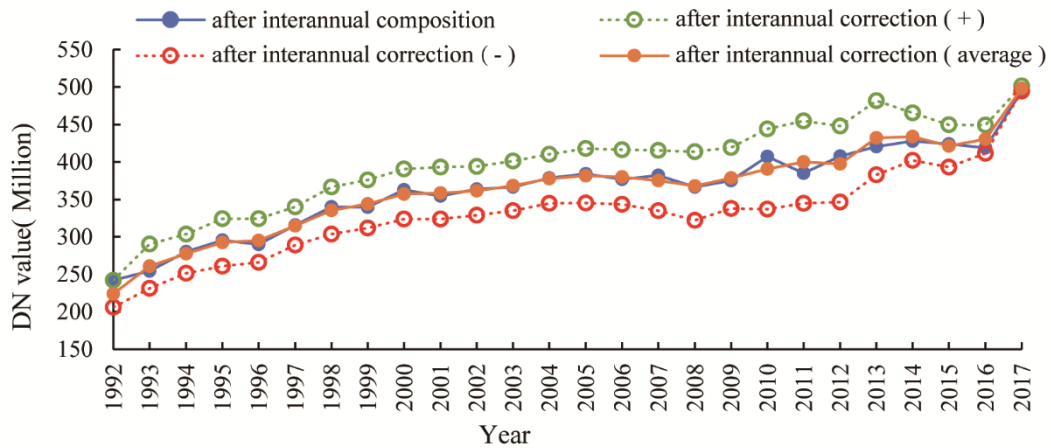


Figure S1. The annual sums of the DN values of the DMSP-OLS and NPP-VIIRS datasets before and after interannual correction. The positive and negative deviations cancel each other based on the correction method proposed by Zhao et al. [7]. The corrected and input annual data deviate very little and essentially show a steady increase.

References

- 1 Ji, G., Zhao, J., Yang, X., Yue, Y. & Wang, Z. Exploring China's 21-year PM10 emissions spatiotemporal variations by DMSP-OLS nighttime stable light data. *Atmospheric environment* **191**, 132-141 (2018).
- 2 Li, X. & Zhou, Y. A stepwise calibration of global DMSP/OLS stable nighttime light data (1992–2013). *Remote Sensing* **9**, 637 (2017).
- 3 Liu, Z., He, C., Zhang, Q., Huang, Q. & Yang, Y. Extracting the dynamics of urban expansion in China using DMSP-OLS nighttime light data from 1992 to 2008. *Landscape and Urban Planning* **106**, 62-72 (2012).
- 4 Li, X., Li, D., Xu, H. & Wu, C. Intercalibration between DMSP/OLS and VIIRS night-time light images to evaluate city light dynamics of Syria's major human settlement during Syrian Civil War. *International Journal of Remote Sensing* **38**, 5934-5951 (2017).
- 5 He, C. *et al.* Restoring urbanization process in China in the 1990s by using non-radiance-calibrated DMSP/OLS nighttime light imagery and statistical data. *Chinese Science Bulletin* **51**, 1614-1620 (2006).

- 6 Liu, L. & Leung, Y. A study of urban expansion of prefectural-level cities in South China using night-time light images. *International Journal of Remote Sensing* **36**, 5557-5575 (2015).
- 7 Zhao, N., Zhou, Y. & Samson, E. L. Correcting incompatible DN values and geometric errors in nighttime lights time-series images. *IEEE Transactions on Geoscience and Remote Sensing* **53**, 2039-2049 (2014).

Supplementary Material 2

Regionalization scheme in the regional scale analysis

1. The World Bank's global zoning scheme

Table S1. Countries by region (from the World Bank).

Regions	Countries	Area (km ²)	Number of countries
East Asia and the Pacific (EAS)	American Samoa, Australia, Brunei Darussalam, Cambodia, China, Fiji, French Polynesia, Guam, Indonesia, Japan, Kiribati, Korea, North Korea, Lao PDR, Malaysia, Marshall Islands, Micronesia, Mongolia, Myanmar, Nauru, New Caledonia, New Zealand, Northern Mariana Islands, Palau, Papua New Guinea, Philippines, Samoa, Singapore, Solomon Islands, Thailand, Timor-Leste, Tonga, Tuvalu, Vanuatu, Vietnam	33737757 (15.3%)	35
Europe and Central Asia (ECS)	Albania, Andorra, Armenia, Austria, Azerbaijan, Belarus, Belgium, Bosnia and Herzegovina, Bulgaria, Channel Islands, Croatia, Cyprus, Czech Republic, Denmark, Estonia, Faroe Islands, Finland, France, Georgia, Germany, Gibraltar, Greece, Greenland, Hungary, Iceland, Ireland, Isle of Man, Italy, Kazakhstan, Kosovo, Kyrgyz Republic, Latvia, Liechtenstein, Lithuania, Luxembourg, Moldova, Monaco, Montenegro, Netherlands, North Macedonia, Norway, Poland, Portugal, Romania, Russian Federation, San Marino, Serbia, Slovak Republic, Slovenia, Spain, Sweden, Switzerland, Tajikistan, Turkey, Turkmenistan, Ukraine, United Kingdom, Uzbekistan	71045721 (32.1%)	58
Latin America and the Caribbean (LCN)	Antigua and Barbuda, Argentina, Aruba, Bahamas, Barbados, Belize, Bolivia, Brazil, British Virgin Islands, Cayman Islands, Chile, Colombia, Costa Rica, Cuba, Curacao, Dominica, Dominican Republic, Ecuador, El Salvador, Grenada, Guatemala, Guyana, Haiti, Honduras, Jamaica, Mexico, Nicaragua, Panama, Paraguay, Peru, Puerto Rico, Sint Maarten (Dutch part), St. Kitts and Nevis, St. Lucia, St. Martin (French part), St. Vincent and the Grenadines, Suriname, Trinidad and Tobago, Turks and Caicos Islands, Uruguay, Venezuela, Virgin Islands (U.S.)	25615298 (11.6%)	42
Middle East and North Africa (MEA)	Algeria, Bahrain, Djibouti, Egypt, Arab Republic, Iran, Islamic Republic, Iraq, Israel, Jordan, Kuwait, Lebanon, Libya, Malta, Morocco, Oman, Qatar, Saudi Arabia, Syrian Arab Republic, Tunisia, United Arab Emirates, West Bank and Gaza, Yemen	14449227 (6.5%)	21
North America (NAC)	Bermuda, Canada, United States	40465437 (18.3%)	3
South Asia (SAS)	Afghanistan, Bangladesh, Bhutan, India, Maldives, Nepal, Pakistan, Sri Lanka	6598583 (2.98%)	8
Sub-Saharan Africa (SSF)	Angola, Benin, Botswana, Burkina Faso, Burundi, Cabo Verde, Cameroon, Central African Republic, Chad, Comoros, Democratic Republic of Congo, Cote d'Ivoire, Equatorial Guinea, Eritrea, Eswatini, Ethiopia, Gabon, Gambia, Ghana,	29218214 (13.2%)	48

Guinea, Guinea-Bissau, Kenya, Lesotho, Liberia, Madagascar, Malawi, Mali, Mauritania, Mauritius, Mozambique, Namibia, Niger, Nigeria, Rwanda, Sao Tome and Principe, Senegal, Seychelles, Sierra Leone, Somalia, South Africa, South Sudan, Sudan, Tanzania, Togo, Uganda, Zambia, Zimbabwe

2. The administrative regions, provinces or states of the countries included in the key areas

Table S2. Significantly changed global lighting clustered areas.

Number	Regions	Districts
1	Eastern and coastal China (CES)	Beijing, Tianjin, Chongqing, Shanghai, Hebei, Henan, Shandong, Shanxi, Anhui, Hubei, Hunan, Jiangsu, Jiangxi, Shanxi, Zhejiang, Fujian, Guangdong, Guizhou (20)
2	Southeast Asia (SEA)	Myanmar, Thailand, Laos, Vietnam, Cambodia, Malaysia, Indonesia (7)
3	South Asia (SAS)	India, Pakistan, Sri Lanka (3)
4	Around the Persian Gulf (PGA)	United Arab Emirates, Iran, Iraq, Kuwait, Oman, Atal, Saudi Arabia (7)
5	Along the Mediterranean (MRA)	Albania, Algeria, Egypt, Syria, Bulgaria, Morocco, Macedonia, Bosnia and Herzegovina, France, Montenegro, Kosovo, Croatia, Lebanon, Libya, Romania, Portugal, Serbia, Cyprus, Slovenia, Tunisia, Turkey, Spain, Greece, Israel, Italy, Jordan (26)

Supplementary Material 3

Regional division and statistics of each region 1. Determination of the Partition Threshold

The brightness, pixel frequency, and cumulative probability statistics for the global nighttime lights were calculated, and the world was divided into a low-brightness zone (LBZ), a medium-brightness zone (MBZ), and a high-brightness zone (HBZ). First, according to the frequency distribution characteristics of the brightness of all pixels (excluding the zero-value pixel) in 1992, the cumulative probability was divided into three segments, namely, 0~33%, 34%~66%, and 67%~100%, and the corresponding nighttime light DN values were approximately 0~6, 6~10, and 10~63, respectively. Finally, the lighting thresholds of the above three types of areas were determined as follows: LBZ: (0,6), MBZ: (6,10), and HBZ: (10~63).

When quantifying the area of these three types of lighting zones, the global largest lighted area was first determined based on all the lighting data from 1992 to 2017. Thereafter, within the maximum lighted area, the specific spatial locations of the above three types of areas were determined in the different years.

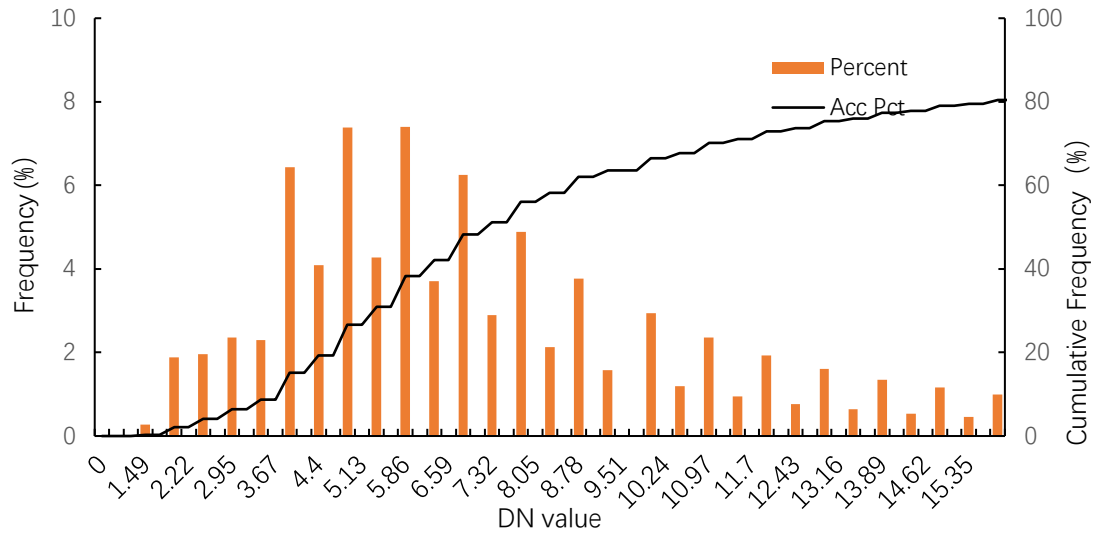


Figure S1. Frequency distribution of the DN value of the nighttime lights.

2. Partition Results

- (1) The TNL of central and eastern coastal China (CEC) increased from 0.07×10^8 in 1992 to 0.32×10^8 in 2017, and the annual growth rate of the TNL reached 6.3%. Compared to 1992, 63.5% of the lighted area brightened, and 1.6% of the lighted area darkened. The total TNL increase was 0.25×10^8 , which is equivalent to 0.30 times the TNL of the United States in 2017. The total brightened area was $0.15 \times 10^7 \text{ km}^2$, which is equivalent to 0.1 times the size of the United States.
- (2) The TNL of the Southeast Asia region (SEA) increased from 0.02×10^8 in 1992 to 0.14×10^8 in 2017, and the annual growth rate of the TNL reached 8.0%. Compared to 1992, 50.6% of the lighted area became brighter, and 1.5% of the lighted area became darker. The total TNL increase was 0.12×10^8 , which is equivalent to 0.15 times the TNL of the United States in 2017. The total brightened area was $0.07 \times 10^7 \text{ km}^2$, which is equivalent to 0.04 times the size of the United States.
- (3) The TNL of the South Asia region (SAS) increased from 0.10×10^8 in 1992 to 0.44×10^8 in 2017, and the annual growth rate of the TNL reached 6.2%. Compared to 1992, 64.0% of the lighted area brightened, and 3.0% of the lighted area darkened. The total TNL increase was 0.34×10^8 , which is equivalent to 0.41 times the TNL of the United States in 2017. The total brightened area was $0.22 \times 10^7 \text{ km}^2$, which is equivalent to 0.14 times the size of the United States.
- (4) The TNL of the Persian Gulf (PGA) increased from 0.08×10^8 in 1992 to 0.29×10^8 in 2017, and the annual growth rate of the TNL reached 5.3%. Compared to 1992, 56.8% of the lighted area became brighter, and 2.2% of the lighted area became darker. The total TNL increase was 0.21×10^8 , which is equivalent to 0.25 times the TNL of the United States in 2017. The total brightened area was $0.11 \times 10^7 \text{ km}^2$, which is equivalent to 0.07 times the size of the United States.
- (5) The TNL of the Mediterranean (MRA) increased from 0.25×10^8 in 1992 to 0.62×10^8 in 2017, and the annual growth rate of the TNL reached 3.7%. Compared to 1992, 52.5% of the lighted area brightened, and 3.6% of the lighted area darkened. The total TNL increase was 0.37×10^8 , which is equivalent to 0.44 times the TNL of the United States in 2017. The total brightened area was $0.26 \times 10^7 \text{ km}^2$, which is equivalent to 0.16 times the size of the United States.